Overview of Results obtained at the Globus-M Spherical Tokamak

V.K. Gusev 1), S.E. Aleksandrov 1), V.Kh. Alimov 2), I.I. Arkhipov 2), B.B. Aushin 1), A.G. Barsukov 3), B.Ya. Ber 1), F.V. Chernyshev 1), I.N. Chugunov 1), A.V. Dech 1), V.E. Golant 1), A.E. Gorodetsky 2), V.V. Dyachenko 1), M.M. Kochergin 1), A.A. Kurdumov 4), G.S. Kurskiev 1), S.A. Khitrov 1), N.A. Khromov 1), V.M. Lebedev 5), V.M. Leonov 3), N.V. Litunovstky 6), I.V. Mazul 6), V.B. Minaev 1), A.B. Mineev 6), M.I. Mironov 1), I.V. Miroshnikov 7), E.E. Mukhin 1), Yu.A. Nikolaev 1), A.N. Novokhatsky 1), A.A. Panasenkov 3), M.I. Patrov 1), M.P. Petrov 1), Yu.V. Petrov 1), K.A. Podushnikova 1), V.A. Rozhansky 7), V.V. Rozhdestvensky 1), N.V. Sakharov 1), O.N. Shcherbinin 1), I.Yu. Senichenkov 7), A.E. Shevelev 1), E.V. Suhov 4), I.N. Trapesnikova 1), E.I. Terukov 1), G.N. Tilinin 3), S.Yu. Tolstyakov 1), V.I.Varfolomeev 1), A.V. Voronin 1), A.P. Zakharov 2), R.Kh. Zalavutdinov 2), V.A. Yagnov 8), E.A. Kuznetsov 8), E.G. Zhilin 9)

1) Ioffe Physical-Technical Institute of the Russian Academy of Sciences, St.Petersburg, Russia
2) A.N.Frumkin Institutes of Physical Chemistry and Electrochemistry, Russian Academy of Sciences, Moscow, Russia
3) NFI RRC “Kurchatov Institute”, Moscow, Russia
4) St. Petersburg State University, St.Petersburg, Russia
5) B.P.Konstantinov Nuclear Physics Institute, Russian Academy of Science, Gatchina, Russia
6) D.V.Efremov Institute of Electrophysical Apparatus, St.Petersburg, Russia
7) Saint Petersburg State Polytechnical University, St. Petersburg, Russia
8) State Research Center of Russian Federation, TRINITI, Moscow region, Troitsk, Russia
9) Ioffe Fusion Technologies Ltd., St. Petersburg, Russia

e-mail contact of main author: vasily.gusev@mail.ioffe.ru

Abstract. Experiments and simulations to achieve high values of plasma parameters at the Globus-M spherical tokamak (ST) at moderate auxiliary heating power (0.2 - 0.8 MW) are described. Important distinguishing features are the low edge safety factor range, which is unusual for spherical tokamaks, $2.7 < q < 5$ and small plasma-outer wall space (3-5 cm). High ion heating efficiency with NB injection was demonstrated. Results of numerical simulation of fast ion trajectories are described and fast ion generation during NB injection and ICR heating is discussed. Also results on their confinement and slowing down processes investigation are presented. Reasons for achievement of high IC heating efficiency are outlined. Reliable H-mode regime achievement is described. Transport ASTRA modeling demonstrated that during NB heated H-mode ion heat diffusivity remains neoclassical and the particle diffusion coefficient inside transport barrier decreases significantly. RGTi divertor tile analysis was performed after irradiation by plasma during big number of shots (10000 shots in average). Mixed layer composition is measured and deuterium retention in different tokamak first wall area is estimated. Plasma jet injection experiments with upgraded plasma jet are described. Jet penetration to the plasma center with immense increase of density and temperature drop is proved and analogy with pellet injection is outlined.

1. Introduction

Globus-M is one of modern STs concentrating its program onto the most significant branches of hot temperature plasma research, with application to fusion devices. Detailed attention is devoted to development of plasma auxiliary heating methods, investigation of heating physics, transport and plasma MHD stability study. Diagnostics and fuelling tools development, investigation of plasma-wall interaction aimed to material research and creation of the basis for noninductive CD are also important parts of the research program. Basic Globus-M features and basic results could be found in [1-9].
The current report is devoted to overview of results achieved on Globus-M for the period since 21st IAEA FEC 2006 up to now. During the reported period further improvement of the device performance has been made. Basic efforts were devoted to increase of target plasma parameters, to

NBI system improvement, heating physics clarification in ST conditions, H-mode study, development of diagnostics, investigation of plasma-wall products and deuterium retention, and the upgrade of the plasma jet injection method for tokamak fuelling purpose.

2. Plasma auxiliary heating and fast ion confinement

The basic plasma auxiliary heating method in Globus-M is the neutral beam (NB) injection of a deuterium or hydrogen atoms. Typical NB parameters are 0.3-0.8 MW of beam power and 20-29 keV of beam energy [9, 10]. The NB heating physics in ST conditions was studied on few machines only [11, 12, 13] and requires further clarification. The second auxiliary heating method is the ion cyclotron resonance (ICR) heating in a frequency range corresponding to the fundamental harmonic of a hydrogen minority in deuterium plasma. Such a method is under the test on STs for the first time. Typical range of ICR parameters is frequency 0.7 - 0.9 MHz and power 0.1 - 0.3 MW [6].
The heating experiments on Globus-M have an important difference as compared to other STs. At first Globus-M is a small dimension tokamak: the plasma major radius is R~0.36 m, the minor radius, a~0.24 m, the aspect ratio, A=R/a~1.5, the plasma vertical elongation $\kappa \sim 1.5 \div 2$. Due to strong toroidicity the toroidal magnetic field changes along the major radius from 1.1 T to 0.23 T from inner to outer border. The typical NB footprint is comparable with plasma cross section. Also the vacuum length of heating wave exited by antenna loop during ICRH exceeds the plasma dimensions. Moreover, at such conditions fast particle orbits span over a wide plasma region. Such sophistications make heating physics investigation of primary importance. Secondary in Globus-M specific heating power deposition could reach high value of $2 \div 3$ MW/m^3. And finally experiments in Globus-M are ordinary conducted at unusually low (for STs) safety factor range $2.7 < q_{95} < 5$ ($0.8 < q_{cyl} < 1.4$) and small plasma-outer wall gap (3-5 cm).

2.1. NBI heating. During NB heating investigation fast ion performance was studied by charge-exchange (CX) diagnostics. The diagnostics consist of two neutral particle analyzers (NPA) of ACORD type [14]. The equipment arrangement is shown in Fig.1. Chosen NPA arrangement provided data about trapped ions ($\perp$ NPA ACORD-12), as well as about passing ions (// NPA ACORD-M) and made possible study of fast ions generated during NB and ICR heating experiments [15]. Estimates predict noticeable first orbit and shine through losses of the beam ions in a low toroidal magnetic field and in small size plasma at low plasma density. Experiments to study deceleration physics of NB produced fast ions were performed. The slowing down energy spectra measured during NB co-injection into deuterium plasma are shown in Fig.2. Solid line corresponds to the theoretical prediction of slowing down due to coulomb collisions [16]. Particle flux steps at energies $E_b/2$ and $E_b/3$ are clearly defined. Direct losses were estimated on the basis of beam particle trajectory simulations [17] and were taken into account. The magnetic field geometry was reconstructed from magnetic measurements with the EFIT code [18]. The spectra waveforms (Fig.2) well correspond to the fundamental coulomb collision slowing down process with corrections to the direct beam ion loss prediction (20 % for H-beam and 40 % for D-beam). In spite of difficulties mentioned above and relatively high beam ion losses predicted at low target plasma

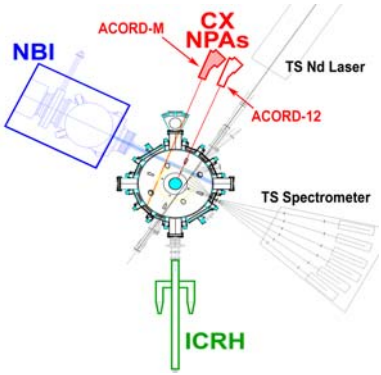

FIG. 1. Apparatus arrangement at the Globus-M tokamak.

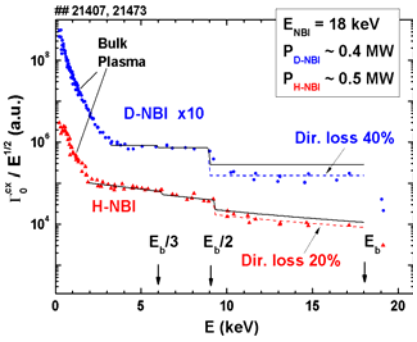

FIG. 2. Slowing down energy spectra measured during H-NBI and D-NBI

densities [10], high ion heating efficiency was demonstrated in Globus-M. With NB power $P_{NB} = 0.8$ MW and $E_b = 25$ keV ion temperature increased ~3.5 times from the OH value and reached 0.75 keV value during NB injection (Fig.3). In this experiment the ion temperature is 1.5 times greater than electron temperature. Later on the experiment with "overheated" ions was repeated in other conditions. Direct beam orbit losses were decreased two times due to the shift of plasma column towards the inner wall by ~ 5cm. The ion temperature increase during shifted plasma NB heating is about 2.5 times higher than in normal (non shifted) column [15]. Numerical orbit simulation shows that currently NB generated fast D^+ ions with the energy up to 25 keV could be confined inside a wide region of plasma in Globus-M. The maximal energy of confined ions during co-injection is limited in conditions of Globus-M (plasma current 200 kA) by high energies 50-70 keV. However high energy ions are confined in quite narrow zone and experience high losses outside it, [19] and further optimization of NB heating in Globus-M is desirable. Nonetheless, NB heating produces high energy content and improves MHD stability of Globus-M plasma. Temporal evolution of plasma parameters in one of the record shots is shown in Fig. 4.

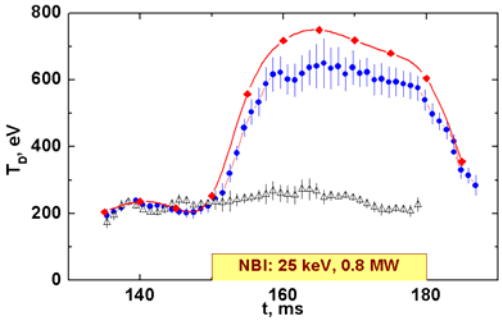

FIG. 3. Record ion temperature during NBI heating in Globus-M. ● - Measured by NPA, ♦ - Corrected to plasma opacity.

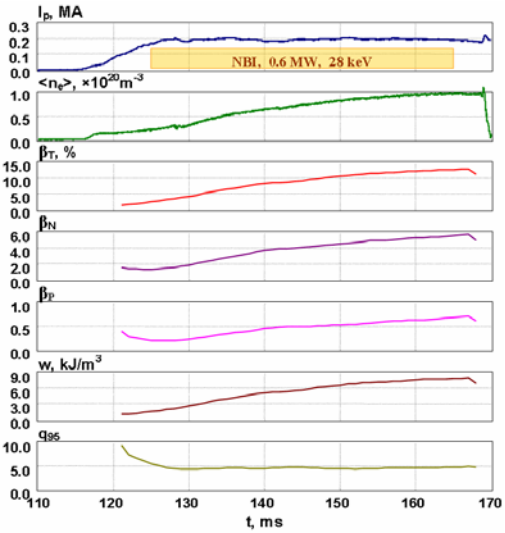

FIG. 4. Temporal evolution of plasma parameters in the Globus-M shot with record values of stored energy and beta normalized.

2.2. Ion cyclotron heating. ICR heating experiments at the fundamental harmonic of light atomic mass (hydrogen) minority in deuterium plasma were performed in the Globus-M spherical tokamak. Such a heating scheme was used in spherical tokamaks for the first time. Wide range of "minority" concentration in deuterium plasma, $n_H/(n_H+n_D) \approx 10$-70% is a specific feature of Globus-M experiments. Experiments with single loop antenna launcher, exciting broad spectrum (N<150) were performed and results were compared with numerical simulations of fast magneto-sonic wave propagation and absorption in Globus-M [6]. It has been found that at optimized experimental conditions, which require displacement of second harmonic resonance beyond the launcher, presence of reflecting walls, surrounding antenna and big power fraction launched into the short wave part of the antennae spectrum the heating efficiency is high enough. Doubling of ion temperature at 200 kW of launched power could be achieved at high "minority" concentration [6].

The absorption of fast magnetosonic waves in plasma is accompanied by generation of hydrogen suprathermal

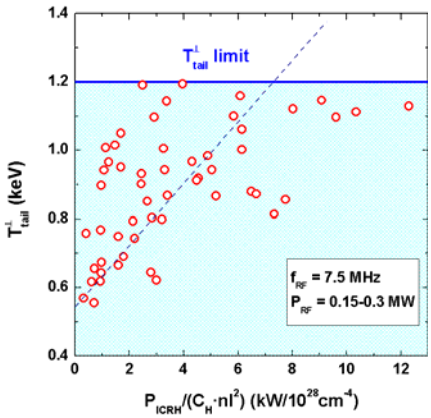

FIG. 5. ICRH "tail" temperature dependence on the specific power deposition per single particle. Dashed line theory "tail" - temperature dependence at $P_{ICRH}/C_H\, nl^2 > 1$, solid line - experimentally observed "tail" temperature limit.

ions. CX energy spectrum of light atomic mass minority (hydrogen) analysis reveals that it consists of two parts. One represents the thermal part and another one is so called high energy tail. Due to the tail slope one could define the tail "temperature". According to classic ICR heating theory, developed for conventional tokamaks, the tail temperature is linearly dependent on Stix parameter [20, 21]. This is not the case in ICR heating in ST. In our experiments RF power input per single particle (roughly Stix parameter) was changed by the factor of 25. At the same time the tail temperature changed only two times and remained below 1.2 keV. The experimental data are presented in Fig.5. The dashed line show theoretical prediction for conventional tokamak, the solid one is the experimental limit in the case of Globus-M. It indicates that the RF power absorbed by minority ions from the tail is limited. We assumed that this limitation was connected with finiteness of energy of accelerated minority ions. In other words the minority ions undergo first orbit losses if they exceed some maximal energy E_{max}. Using the observation of CX flux decay after RF termination, the maximal energy of accelerated protons was estimated as E_{max}~ 15 keV [15]. To prove the experimental data trajectory simulations of minority ions in the Globus-M magnetic field, reconstructed using the EFIT code, were performed. Figure 6 demonstrates the fast ion banana orbit (left) and the map of banana orbit tip positions for different E_{max} (right). Solid oval line indicates the plasma last closed flux surface (LCFS). ω_H line shows the position of the cyclotron resonance for the hydrogen fundamental harmonic ω_H. This map could be regarded as zones of fast proton confinement in Globus-M poloidal cross-section born with different energies. As can be seen E_{max} is about 15 keV for protons having the banana orbit tips near the fundamental harmonic region. This correlates well with the value estimated from experiment. One should keep in mind that in the Globus-M condition considerable part of FMS wave power can be transmitted to plasma ions without producing ion tails through Bernstein wave conversion. This may partly explain the heating efficiency increase especially at higher hydrogen concentration.

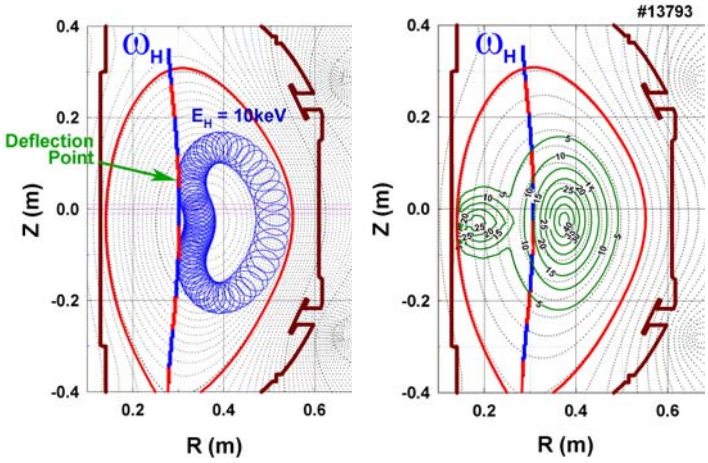

FIG. 6. Left - Banana trajectory of 10 keV proton Right – Zones of different energy fast protons confinement (labeled). Solid red (oval) – LCFS. ω_H - IC resonance position for H^+.

3. High plasma confinement regime

Reliable transition into high confinement regime (H-mode) was achieved in Globus-M after changing of the toroidal magnetic field direction. The toroidal magnetic field became parallel to the plasma current direction. Ion ∇B drift is directed towards the lower X-point, which is usually placed inside vacuum vessel. L-H transitions are recorded in OH regime, in NB and IC heating regimes both in limiter and divertor configurations. Different events could trigger the H-mode (MHD, gas puff, etc.) [22]. The change of the toroidal magnetic field direction also improved the plasma performance in the L-mode. Radiation losses decreased two times, plasma internal inductance decreased ~20%, loop voltage decreased ~20÷30% accompanied by some increase of the plasma energy content. The possible reasons can be connected with the spontaneous reduction of error magnetic fields after toroidal field redirectioning.

3.1. Ohmic H-mode. Temporal evolution of plasma parameters in ohmic H-mode, shot #21987, is shown in Fig. 7. The L-H transition took place in the initial phase of the plasma discharge, triggered by gas puff reduction. In the phase of the transition the OH power does not exceed $P_{OH} \leq 0.3$ MW. Transition is followed by a formation of a steep gradient in the electron density profile near the separatrix and a flat density distribution over the plasma volume. Sometimes characteristic "ears" are formed on the density profile at the initial stage of the H-mode regime [22].

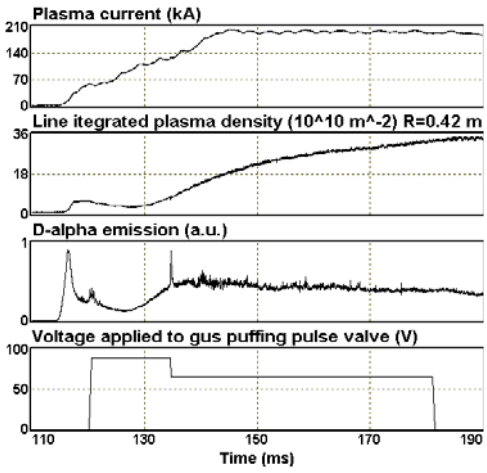

FIG. 7. Time evolution of plasma parameters in OH H-mode. Shot #21987.

Experimentally measured values of the plasma ion and electron temperatures, density and plasma loop voltage were used as the input parameters for the 1D ASTRA code simulations [23]. The transport model is described in [24]. The ion energy transport was simulated by the neoclassical NCLASS code [25], which was incorporated into the ASTRA package. Electron transport coefficients were prescribed. For simulation simplicity the radial χ_e dependence was not included, $\chi_e(r) \sim$const. The transport coefficients were adjusted to provide consistency of the fitted density and temperature profiles and fitted plasma voltage to the experimental data. The measured and simulated density and temperature profiles are shown in Fig.8a and 8b. The resulted transport coefficients providing experimental and simulated data adjustment are shown in Fig.9. In the figures the normalized minor radius is defined as a_ψ/a_b, where a_ψ is a half-width of a current flux surface in a midplane and a_b is its boundary value. Plasma thermal energy content simulated by ASTRA is in a good agreement with the energy content reconstructed from magnetic measurements with the EFIT code [26]. The plasma thermal energy content reached the value about 2.5 kJ, and the energy confinement time $\tau_E \sim 8 \div 10$ ms. This value is consistent with the ITER scaling IPB98(y,2) [27].

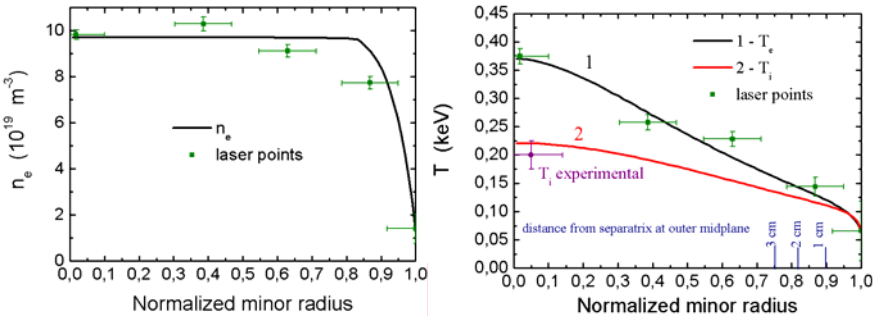

FIG. 8. Measured and fitted electron density and temperature profiles. Shot#21987, quasistationary phase.

3.2. NBI heated H-mode and threshold power estimate. Stable L-H transition was observed during the NB injection. All characteristic H-mode features are demonstrated in NB heated H-mode, including ELMs. During transport analysis it is found out that the same difficulties, which complicate NB heating experiments in Globus-M plasma, are applicable also to the numerical simulations. For simulation of the transport processes in NB heated H-mode the ASTRA code was also used [23]. NBI subroutine was specially revised for the Globus-M tokamak parameters. Typical plasma shot traces in NB heated H-mode discharge # 19518 are shown in Fig.10. The transport simulations were performed with the details presented in [24].

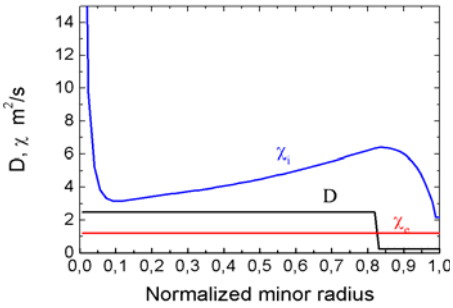

FIG. 9. Simulated transport coefficients in ohmic H-mode. Shot#21987, Time=167 ms.

The major result of transport simulations is that common features of both ohmic and NB heated H-modes are basically the same, i.e. transport barrier is created on the density profile only and is not present on the ion and electron temperature profiles. The particle diffusion is significantly suppressed by the inside transport barrier which is formed near separatrix (~10 times) and particle diffusion coefficients fell down below D~0.6m^2/s during both OH and NB H-modes. Ion transport did not change significantly from L to both H-mode states. It remained neoclassical with χ_i~2÷6 m^2/s across the plasma radius. The strong variation was detected only in electron heat diffusivity. It changed from χ_e~10 m^2/s in the L-mode to ~ 8 m^2/s in NB H-mode and significantly decreased down to ~1.2 m^2/s in ohmic H-mode. A difference in electron heat diffusivity between two H-mode discharges is in qualitative agreement with ITER IPB98(y,2) scaling, $\chi_e \sim 1/\tau_E \sim P_{tot}^{0.69}/n^{0.41}$, since in the NB H-mode density is twice lower and heating power is twice higher. Quantitative agreement is not reached yet and no adequate explanation of discrepancy between electron heat transport coefficients in two H-mode regimes exists. Choosing more sophisticated radial dependence, other than $\chi_e(r)$=const, may decrease disparity, but strong difference between two selected discharges in electron transport will be conserved. Currently due to rather poor transport analysis data base in Globus-M we could not define proper dependence of $\chi_e(r)$, but we can declare the evidence of electron temperature transport barrier absence.

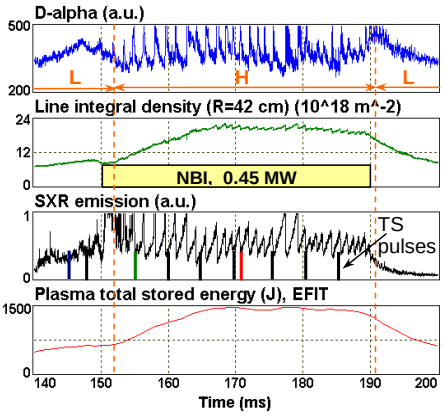

FIG. 10. L-H transition in the NBI heated Globus-M shot # 19518.

The ASTRA code simulation revealed that the L-H transition was accompanied by an increase of the electric field (poloidal rotation) shear in the transport barrier region [28]. The critical shear value is about 10^6 s^{-1}, which is of the order of values typical for ASDEX-Upgrade and MAST [29]. This corresponds to the conception of the turbulent transport suppression. The L-H transition occurs when the heat power absorbed by ions exceeds the transition power threshold. The threshold power for the case of the Globus-M conditions calculated in accordance with the international database [27] is $P_{L-H} \approx 50$ kW. In ohmic H-mode this power may be transferred to ions by electron heat flux at the densities higher than 2×10^{19}m^{-3}. That is the case for the discharge # 21987. In the case of discharge # 19518 the density is lower and the power flux from electrons is insufficient and auxiliary NB power absorbed by ions resolve the threshold problem. Typical power transferred to ions in the L-mode due to electron-ion exchange is below 50 kW at densities referred above in spite of relatively high ohmic power ~ 300 kW [24].

4. Plasma-wall interaction study

A big power flux to the first wall is a feature of the Globus-M tokamak. Keeping in mind high specific power deposition (2÷3 MW/m^3) and power flux "focusing" effect along the magnetic separatrix footprint the power flux density could reach several MW/m^2 on the divertor plates. Also a small gap between plasma and the first wall in Globus-M makes plasma facing material choice a crucial issue. At present about 90% of the in-vessel surface faced to plasma is protected with tiles manufactured from RGTi type of graphite which is doped with 2 at.% of Ti and 0.3-0.7 at.% of Si [30, 31]. Figure 11 shows the first wall picture of Globus-M. Carbo-

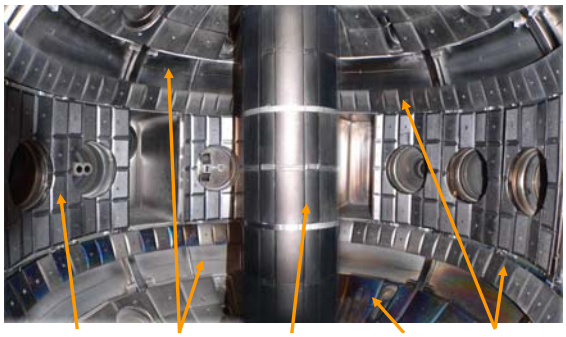

FIG. 11. Plasma-facing surface (first wall) of the Globus-M vacuum vessel.

boronization procedure based on decomposition of dodecarboran powder ($B_{10}C_2H_{12}$) in He glow discharge is used for vessel conditioning [32]. Boron is one of the main components of a primary protective layer deposited onto first wall surfaces and is responsible for impurity and hydrogen isotope absorption [33]. Chemical composition was analyzed and structural-phase analysis was made of the deposits (mixed layers) obtained during primary carbo-boronization procedure and their following modification during plasma-wall interaction in Globus-M.

4.1. Sampling and analysis.

The lower part of the Globus-M poloidal cross-section with a magnetic plasma configuration enclosed is shown in Fig. 12a. Divertor RGTi graphite tiles are marked (1-7). Part of the RGTi tiles and samples (stainless steel) were extracted from the vessel after interaction with plasma. The tiles from the zone of direct plasma fluxes to the wall were exposed during ~10000 discharges (exposition time ~1000 s), the stainless steel samples, installed in "shadowed" zones (screened from direct plasma fluxes), were exposed to 2800 plasma discharges (exposition time ~300 s). Electron probe microanalysis [34], scanning electron microscope and X-ray diffraction methods were used for the analysis. Deuterium depth profiles in layers deposited onto divertor tiles were determined by the $D(^3He,p)^4He$ nuclear reaction in a resonance-like technique with the analyzing beam of ^3He ions (E=0.69-3.2 MeV) together with the computer program SIMNRA [35, 36]. Mixed layers in "shadowed" zone were analyzed by Rutherford backscattering spectrometry and nuclear reaction analysis with an electrostatic accelerator of deuterons (E=1 MeV). The boron/carbon and deuterium/carbon ratios in deposits were determined by comparing alpha and proton particle yields in $^{10}B(d,\alpha)^8Be$ and $^{12}C(d,p)^{13}C$ reactions, respectively. Deuterium upper content limit was estimated from the reaction of $D(d,p)^3H$ [37, 38, 39]. Deuterium release from "shadowed" zone samples was studied by thermal desorption spectroscopy (TDS) [40]. Residual contents of boron, carbon, silicon and titanium in the samples after their annealing during TDS and after mechanical removal of surface films were measured again.

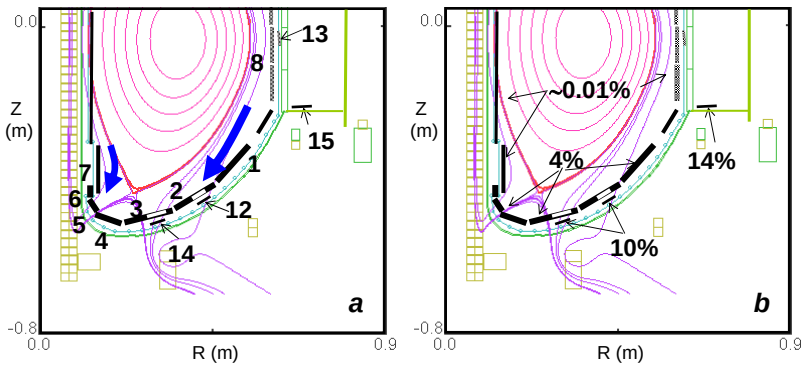

FIG. 12. Left – lower part of Globus-M. Numbered are divertor RGTi tiles and samples exposed to plasma. Right – Deuterium retention coefficient in different areas of the Globus-M first wall.

4.2. Divertor zone analysis results. In the zone exposed to direct plasma fluxes, RGTi divertor tiles did not suffer from destruction. At least inside 10 μm surface layer depth after 3-year of tokamak operation no structural changes were recorded. RGTi material remained in well graphitized and textured mode with a basic plane faced to plasma. Graphite matrix contained also TiC inclusions which were well identified by X-ray diffraction. All the divertor tiles, experienced direct plasma interaction, were covered by mixed layers contained carbon, boron, oxygen and practically all the elements of vessel construction units.

During thermodesorption analysis intensive deuterium release took place in the temperature range 600-900 K (Fig. 13a) which is significantly less than an initial temperature of deuterium release from RGTi graphite exposed to deuterium plasma [40]. This confirmed that deuterium was basically captured by the mixed layers. Deuterium concentration in the divertor tile deposits was not more than 7-8 at.% (i.e., ~10^{18} D/cm^2) after 10000 tokamak pulses [41]. Minimal deuterium concentration corresponded to the maximal power flux zone. Deuterium concentration in the bulk of RGTi tiles did not exceed 2×10^{-3} at.%.

4.3. Zone "shadowed" from direct plasma fluxes to the wall.
In the "shadowed" zones, which were screened from direct plasma flows, deposits were characterized by well developed surface (Fig. 14). They had a structure typical for hydrogenated amorphous carbon. Except basically amorphous carbon phase the deposit also contained particles of well graphitized carbon, titanium carbide (TiC) and iron oxide (Fe_2O_3). The layers also contained main stainless steel components (Fe, Cr, Ni) as well as O, Si and Ti. Boron concentration in the deposits was lower than carbon one. Deposits accumulated a significant amount of deuterium. The data on the deuterium accumulation in deposits are presented in the Table. The data due to nuclear resonance analysis (NRA) and thermodesorption (TDS) data are presented at the left. On the right in the same table carbon and boron areal density in mixed layers before/after annealing at 1100 K are presented due to electron probe microanalysis (EPMA) data.

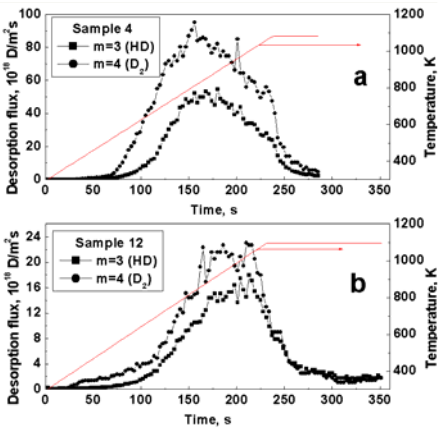

FIG. 13. (a) – Deuterium thermodesorption spectrum for the divertor tile 4.
(b) – Deuterium thermodesorption spectrum for the deposit on sample 12. Linear heating rate is 3.2 K/s

TABLE. THE MAIN ELEMENTS OF DEPOSITED LAYERS.

Sample	Deuterium content, 10^{16} at/cm^2		C, 10^{16} at/cm^2	B, 10^{16} at/cm^2
	NRA data	TDS data (released D_2)	EPMA data before/after annealing	
12	<200	46	165/80	165/31
14	<125	56	86/25	186/17
15	<43	15	36/10	36/16

In spite of intensive deuterium release which was started at 600-700 K (Fig. 13b), only part of the trapped deuterium was desorbed during TDS process (Table - middle). Subsequent analysis of the annealed samples showed that the deposits were partly sublimated (Table – right) and part of deuterium was released as volatile compounds with boron and carbon.
Deuterium retention estimate was made relying upon the presented data. The retention coefficient (the ratio of the captured to the total deuterium amount injected during each tokamak pulse) in Globus-M is R_{ef}~28%. This does not contradict the data obtained from other tokamaks 3-30% [42]. The deuterium retention coefficient for different in-vessel zones is the following: in the "shadowed" zone deposits, R_{ef}~14% (half of the captured deuterium); inside vessel port deposits, R_{ef}~10%; in the zone exposed to direct plasma fluxes, R_{ef}~4%. The deuterium retention is attributed to different areas indicated in Fig. 12b.
Main processes of protective carbon-boron layer modification inside the Globus-M tokamak equipped for the first time by RGTi graphite manufactured are described in [43-45]. The complex mixed layers formed from protective carbon-boron layers and in-vessel component elements are amorphous and trap deuterium.

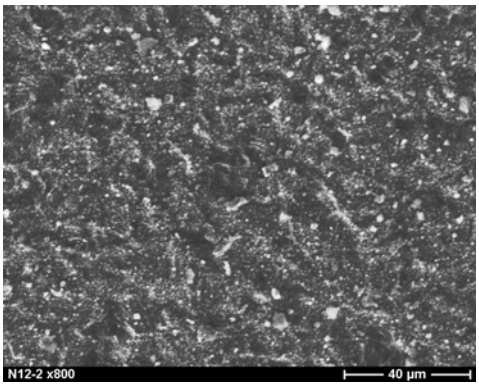

FIG. 14. Scanning electron microscope micrograph of the deposit on the sample 12. The deposit surface is quite rough.

Deuterium is easily released from amorphous noncrystalline layers at moderate heating temperature (700-800 K) or under intensive plasma fluxes partly in the form of volatile boron or carbon compounds, in crystalline layers much higher temperature is required for deuterium release [46].

5. Central fuelling of plasma column

The fuelling method of high speed, high density plasma jet injection is developed at Globus-M. Two stage plasma gun, with explosive method of gas feeding of a coaxial accelerator permits to combine necessary merit of the fuel injector – high density and speed of the jet with high purity of the substance [47]. The mechanism of the jet penetration through magnetic field was proposed, and a deep penetration into tokamak plasma (far beyond separatrix) was demonstrated [48].

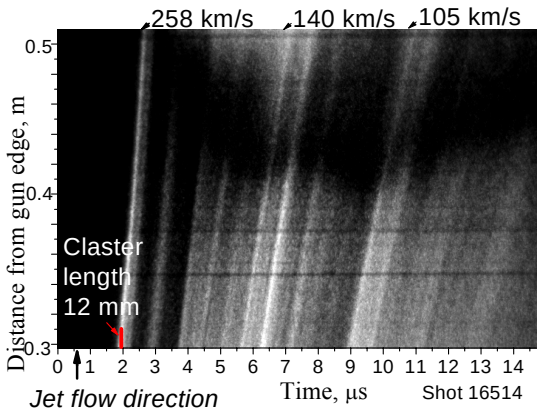

FIG. 15. Streak camera frame of the jet radiation observed through a narrow slit; shot 13898 – perpendicular view.

5.1. Experiments on high speed jet injection into Globus-M. The following jet parameters were achieved in a test bench experiments: maximal density more than 2×10^{22} m^{-3}, total number of accelerated particles $(1\text{-}5)\times10^{19}$. The jet energy measured with a calorimeter increased to 200 J. The jet speed was measured by streak-camera jet radiation recording. Figure 15 shows the image sweep across the sleet of jet propagating along the slit away from the gun muzzle. One can see that the plasma jet consists of several fractions, each of them propagating with its own velocity from 100 to 250 km/s according to different slopes of the strips. The presence of intensive impurity lines radiation is not recorded with a survey spectrometer.

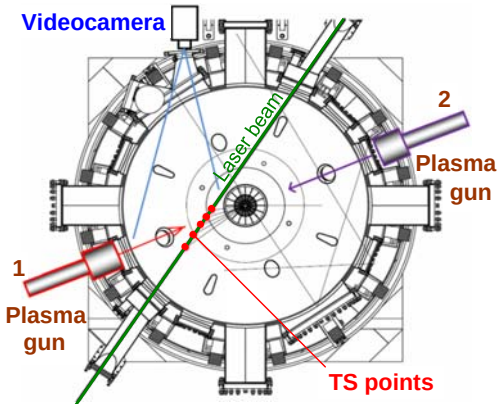

FIG. 16. Horizontal Globus-M cross-section. Red circles are TS measurement points.

Experiments on Globus-M were carried out at two different plasma gun positions shown in Fig. 16. The target plasma parameters were: the plasma current, I_p=200 kA, the toroidal field, B_T=0.4 T, the average density, $\langle n\rangle=(2\text{-}5)\times10^{19}$ m^{-3}. The plasma jet was injected from the low field side in the major radius direction, through a ports (marked by 1 and 2 at Fig.16) placed in the equatorial plane. The Thomson laser beam, spatial laser points at which measurements were taken, the video camera position are also shown. The port 2 is shifted by 180 degrees in toroidal direction from the cross section, where temperature and density measurements were made. Electron temperature and density profiles evolution prior and after jet injection into the Globus-M target plasma was picked up by a high repetition rate Thomson scattering diagnostic [49, 50]. The closest in time measurements were carried out at delay of 35 μs between jet injection and laser shot, reliable profile measurements were carried out at the delay of 50 μs. At short delay between injection and measurements, local temperature and density measurements may be different from the values averaged over the magnetic surface (the case of jet injection from port 1). When the jet was injected from port 2 (180 degrees toroidally from TS points), the magnetic surface averaged values were measured.
The pair of temperature and density profiles just prior the gun shot and 50 μs after it (port 1) is shown in Fig.17a (upper plots) and for the port 2 Fig.17b (lower plots). It is seen that already in 50 μs after the gun shot the electron density increases and temperature drops approximately twice in

both cases. The target plasma density scan was made too. The jet better penetrates to the target plasma with lower density. At $n_e(0)=5\times10^{19}$ m^{-3} the temperature dropped and density grew in the central points (R=38.6, 30.6 cm) more than twice in 50 μs after injection, while at $n_e(0)=8\times10^{19}$ m^{-3} the change was by 20-30 % only.

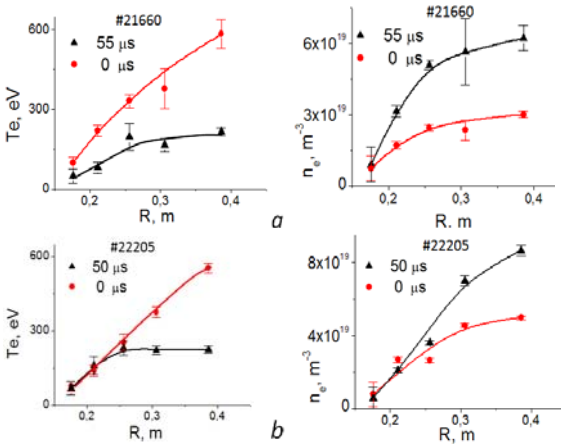

FIG. 17. Electron density and temperature profiles measured before and shortly after the jet injection, in cross section near the gun (upper pictures, shot #21660) and in remote cross section (lower pictures, shot #22205).

5.2. Modeling, objectives and prospects. Jet penetration depth was estimated on the basis of the analytical model using the same approach as was developed for pellet injection simulations. The numerical simulation was performed with the code described in [7]. It is demonstrated that at t=0.9 μs, when jet reaches the plasma centre the drop in the electron temperature is immense. While the electron temperature is dropped almost immediately, the density homogenization over the flux surface is much slower and is determined by the sound speed with the jet temperature. Estimated time for the density homogenization is less than 100 μs. The penetration depth to the tokamak plasma grows with increase of the jet velocity and jet density.

During single jet injection pulse, about 20% of the injected particles are captured into tokamak plasma in Globus-M. Consequences of the plasma jet injection effect are strongly dependent on the injected particle fraction with respect to target plasma inventory. Too high injected particle number led to sharp rise of the target plasma density (up to three times) accompanied by even stronger temperature drop that led to the discharge disruption. At a moderate number of injected particles, the density increase up to two times was observed, accompanied by corresponding temperature drop. Plasma column could decrease its MHD stability at that, resulting sometimes in a locked mode development (usually m=2/n=1) through a sufficiently large time after injection (more than 3 ms). At a small jet particle number, when the density increased no more than by 50 % and the temperature dropped no more than twice the plasma remained MHD stable. In all three described cases, the plasma jet penetrated to the tokamak center that is proved by Thomson measurements and video camera observations. Consequently a right choice of the jet parameters makes it possible to grow the column particle number and control the density profile in a discharge, realizing the main particle contribution to the central or peripheral zone. No essential impurities coming in either with the jet, or due to its interaction with tokamak injection port, were recorded. The jet injection did not affect the global characteristics of the tokamak discharge such as plasma current and loop voltage.

Analogy may be done between the plasma jet and pellet injection. In both cases, the penetration ability depends on speed and density of the injected object, and the influence degree to the target plasma is defined by total number of injected particles. At that, decreasing of the particle density in the plasma jet (10^{21}-10^{22} m^{-3}) by one-two orders of magnitude in comparison with the particle density in the cloud surrounding the pellet (10^{23}-10^{24} m^{-3}), is compensated by the corresponding velocity increase. During a pellet injection the spreading of the gas cloud along the magnetic field takes place [51]. In the plasma jet injection experiments also the gas cloud spreading along the magnetic field lines is detected and coincidence of the shape of protuberances spreading along the field with the pitch angle and curvature of the magnetic field lines in the central region of plasma is shown [52].

6. Conclusions

During auxiliary heating at Globus-M MHD stable plasma regimes with high value of specific energy content (up to 8 kJ/m^3) and high beta normalized ($\beta_N \approx 6$ % m·T/MA) were achieved at moderate heating power (<0.8 MW). Fast particle behavior was investigated and their generation, confinement and slowing down in the conditions of low magnetic field during NB injection and ICR heating was clarified. Important feature is that most of regimes were achieved at low value of the edge safety factor, which is unusual for spherical tokamaks, $2.7 < q_{95} < 5$ and small plasma-outer wall gap (3-5 cm). Reliable transition to the H-mode regime was obtained. The different types of H-modes are accessed (ohmic, NB heated, ICR heated, etc.) and the threshold power was found to be in accordance with international database. Transport barrier was created for the density and no barrier for ion and electron temperatures were detected. Significant diffusion coefficient drop (~10 times) was estimated in the vicinity of separatrix. Experience of the RGTi graphite utilization in the Globus-M spherical tokamak is positive and connected with its high density, low erosion coefficient and poor deuterium sorption ability. A tool for central plasma fuelling on the basis of dense, high velocity plasma jet injection is developed at Globus-M. Injection of the jet with velocity of 200 km/s leads to nearly instantaneous increase of density in the center of plasma column. The plasma density increase is recorded on the magnetic axis of target plasma with 0.2 MA current and density of $(2 - 5)\times10^{19}$m^{-3} within 35-50 μs after injection started. At the same time electron temperature drops significantly.

The authors would like to thank A.Polevoy and G.Pereversev for their help in ASTRA simulations. This work is supported by the Russian Academy of Science, Ministry of Science and Education, Rosatom (contract H.4a.41.03.08.075) and RFBR grants ## 06-02-08142, 06-02-16709, 06-02-16189, 06-08-00878, 08-02-13537-ofi-c, 08-02-13530-ofi-c, 08-02-00511, 05-08-18044.

Appendix 1 : References

[1] GUSEV V.K. et al., Tech. Phys., **44** (9), 1054 (1999).
[2] IRZAK, M.A., et al., Plasma Physics Reports, **25** (8) (1999) 659.
[3] GUSEV, V.K., et al, Tech. Phys. Lett., **30** (8) (2004) 690.
[4] VORONIN A.V., et al., Nuclear Fusion, **45** (2005)1039–1045.
[5] GUSEV V.K. , et al., Nuclear Fusion, **46** (2006) S584-S591.
[6] SHCHERBININ O.N., et al., Nuclear Fusion, **46** (2006) S592-S577.
[7] ROZHANSKY V. et al. Nuclear Fusion, **46** (2006) 367-382.
[8] GUSEV V.K.et al In Proc of 21st IAEA Fusion Energy Conference 2006 Chengdu, China, OV/P-3.
[9] AYUSHIN B.B. , et al., Plasma Physics Reports **34**(2) (2008) 81-94.
[10] GYSEV V.K., et al., Tech. Phys., **52** (2007), 1127.
[11] AKERS R.J., et al., Nucl. Fusion, **42** (2002) No.2, 122-135.
[12] COX M., et al., Fusion Engineering and Design, 1999, **46**, No. 2-4, 397-404.
[13] ONO M., et al., Nucl. Fusion, **40** (2000) No. 3Y, 557561.
[14] IZVOZCHIKOV A.B., et al., Tech. Physics., **37** (1992) 201.
[15] CHERNYSHEV F.V., et al., Proc. of 35th EPS Plasma Phys. Conf., 9 – 13 June 2008, Hersonissos, Crete, Greece (2008) P-2.097.
[16] SIGMAR D.J., Varenna Course on Phys. of Plasmas Close to Thermonuclear Conditions, 1, Brussels (1980) 271.
[17] CHERNYSHEV F.V., et al., Proc. of 34th EPS Conference on Plasma Phys. Warsaw (2007), 2 - 6 July 2007 ECA Vol.**31F**, P-5.107.
[18] LAO L.L., et al., Nucl. Fusion **25** (1985) 1611.

[19] AYUSHIN B.B., MIRONOV M.I.et al. Proc. Of Zvenigorod conf. On Plasma Phys. & Contr.Fusion, 2007.
[20] STIX T.H., 1975 Nucl. Fusion, **15**, 737-754.
[21] CHANIOTAKIS E.A., SIGMAR D.J., 1993, Nucl. Fusion, **33**, 849-861.
[22] GUSEV V.K., et al., in Proc. of 34th EPS Conference on Plasma Phys. Warsaw (2007), 2 - 6 July 2007 ECA Vol.**31F**, P-1.078.
[23] PEREVERZEV G., YUSHMANOV P.N., Max-Plank IPP report 5/98 (2002).
[24] SAKHAROV N.V. et al., This conference, EX/P5-16.
[25] HOULBERG W.A., et al., Phys. Plasmas **4** (1997)3230.
[26] GUSEV V.K., et al., Tech. Phys. **51** (2006) 987.
[27] ITER Physics Basis. Nucl. Fusion **39** (1999) 2175; Nucl. Fusion **47** (2007) S18.
[28] SENICHENKOV I.YU., et al., in Proc. of 35th EPS Plasma Phys. Conf., 9 – 13 June 2008, Hersonissos, Crete, Greece (2008), P-2.097.
[29] ROZHANSKY V., Contrib. Plasma Phys. **46** (2006) 575.
[30] BURTSEVA T.A., et al., Carbon Materials, Proceedings of 6th International Workshop, Jülich, Germany, 23-24 September, 1993, 49.
[31] GORODETSKY A.E., et al., Fus. Eng. Des. 43 (1998) 129.
[32] SHARAPOV V.M., et al., J. Nucl. Mater. 220-222 (1995) 730.
[33] ALIMOV V.KH., et al., J. Nucl. Mater. 196-198 (1992) 670.
[34] ZALAVUTDINOV R.KH., et al., Microchim. Acta 114-115 (1994) 533.
[35] ALIMOV V.KH., et al., Nucl. Instr. and Meth. B 234 (2005) 169.
[36] MAYER M., SIMNRA User's Guide, Tech. Rep. IPP 9/113, Garching, 1997, and www.rzg.mpg.de/~mam.
[37] TESMER J.R., et al., Handbook of Modern Ion Beam Materials Analysis (Materials Research Society, Pittsburgh, Pa., USA, 1995).
[38] GAVRILOV G.E., et al., Nucl. Instr. and Meth. A515 (2003), N 1-2, 108.
[39] BRAZHKIN V.V., et al., Phys. Rev. B74 (2006), 140502-1 (rapid communications).
[40] ARKHIPOV I.I., et al., J. Nucl. Mater. 271-272 (1999) 418.
[41] GUSEV V.K., et al., Proc. of ICFRM-13, 2007, 000390, Nice, France, p.823.
[42] LIPSCHULTZ B., et al., Nucl. Fusion 47 No 9 (2007) 1189-1205.
[43] ANANIEV A.S., et al., Semiconductors. 2002. Vol. 36. No 8. pp. 941-943.
[44] SAKHAROV N.V., et al., Proc. of 29th EPS Conference on Plasma Physics and Controlled Fusion, Montreux, Switzerland, 17-21 June 2002, P – 5.078-081.
[45] GUSEV V.K. et al., This conference, EX/P4-10.
[46] KIKUCHI Y. et al., In proc. of 13th Int. Conf. on Fusion Reactor Materials, 2007, Nice, France, p. 3790.
[47] VORONIN A.V. et al., Nuclear Fusion **45** (2005) 1039.
[48] GUSEV V.K. et al., Nuclear Fusion **46** (2006) S584–S591.
[49] TOLSTYAKOV S.YU. et al, Technical Physics, 51(2006) 846 – 852.
[50] TOLSTYAKOV S.YU. et al, Proc. of 35th EPS Plasma Physics conference, 9-13 June 2008, Hersonissos, Crete, Greece, P.2-108.
[51] PEGOURIE B. Plasma Phys. and Controlled Fusion 49 (2007) R87-R160.
[52] PETROV YU.V. et al., This conference, EX/P5-8.